

1 Anisotropic charge transport in non-polar GaN quantum wells (QWs): 2 polarization-induced line charge and interface roughness scattering

3 Aniruddha Konar,^{1, a)} Tian Fang,¹ Nan Sun,¹ and Debdeep Jena¹

4 *Department of Physics and Department of Electrical Engineering, University of Notre Dame, Notre Dame,*
5 *USA 46556*

6 (Dated: 1 January 2019)

Charge transport in GaN quantum well (QW) devices grown in the non-polar direction is theoretically investigated. Emergence of a new form of anisotropic line charge scattering mechanism originating from anisotropic rough surface morphology in conjunction with in-plane built-in polarization is proposed. It is shown that such scattering leads to a large anisotropy in carrier transport properties, which is partially reduced by strong isotropic optical phonon scattering.

7 The growth of non-polar m -plane ($1\bar{1}00$) and a -plane
8 ($11\bar{2}0$) GaN has attracted a lot of interest recently^{1,2}.
9 Though the built-in polarization field in traditional
10 polar-GaN (c -plane) has been exploited to achieve dopant
11 free high electron mobility transistors (HEMTs), for optical
12 devices, polarization field plays a negative role due
13 to quantum confined Stark effect (QCSE). Moreover, c -
14 plane GaN-based enhancement-mode (E-mode) HEMTs
15 have very low threshold voltage ($V_{th} \sim 1$ V) due to
16 inherent presence of polarization induced electron gas
17 (2DEG). High threshold voltage ($V_{th} \sim 3$ V) is required
18 for high-voltage switching operations. So the recent trend
19 is to explore optical and transport properties of GaN
20 grown in the non-polar direction. Recently E-mode trans-
21 sistor with high threshold voltage (≥ 2 V) has been
22 achieved³ with non-polar GaN heterojunction.
23 A characteristic feature of non-polar GaN surfaces grown
24 directly on foreign substrates is extended stripe or slate
25 like morphology perpendicular to the c axis^{2,7-10}, regard-
26 less of growth methods. The origin of this rough sur-
27 face morphology has been attributed to i) replication of
28 substrate morphology⁴, ii) extended basal-plane stack-
29 ing faults (BSFs)^{2,7}, and iii) anisotropic diffusion bar-
30 rier of Ga adatoms^{5,6}. This striated morphology has
31 been conjectured qualitatively to be responsible for ex-
32 perimentally observed conductivity anisotropy for bulk
33 GaN films¹¹ as well as thin GaN-QWs¹². No microscopic
34 theory is available in existing literature for a quantitative
35 estimation of this electrical anisotropy. This paper devel-
36 ops a microscopic theory of anisotropic carrier transport
37 in non-polar GaN QWs with a quantitative estimation of
38 the transport anisotropy.

39 Let us consider a thin non-polar GaN QW of thickness
40 a sandwiched between two aluminum nitride (AlN) lay-
41 ers as shown in Fig.1a). A common source of disorder
42 for non-polar GaN QW is striped surface morphology
43 as mentioned in the previous section. We model this
44 rough surface morphology as a local variation of QW
45 thickness (see Fig.1) The variation of QW thickness
46 alone causes local shifts of the conduction band edge,

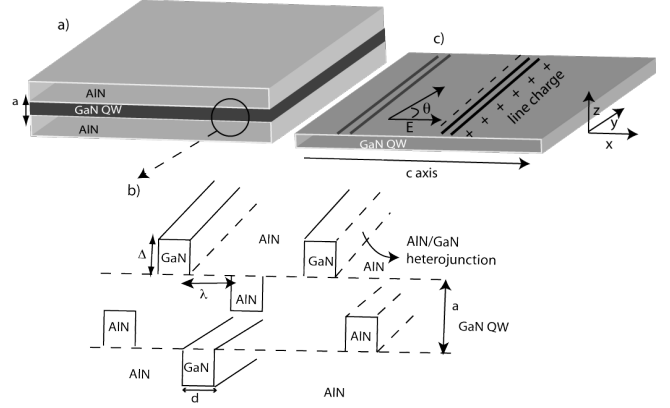


FIG. 1. Non-polar GaN quantum well: a) QW of width a sandwiched between AlN barriers, b) schematic diagram of interface roughness at GaN/AlN interface, c) polarization induced line charge at each step edge of roughness.

48 resulting in carrier scattering commonly known as in-
49 terface roughness scattering (IR) in literature. The in-
50 terface roughness (IR) can be modeled by local thick-
51 ness fluctuations $\Delta(x)$ of the non-polar GaN QW with
52 a spatial correlation $\langle \Delta(x)\Delta(0) \rangle = \Delta^2 \exp[-|x|/\sqrt{2}\Lambda]$,
53 where Δ is the average height of roughness and Λ is
54 the in-plane correlation length between two roughness
55 steps. Denoting the envelope function of conduction elec-
56 trons in the n^{th} subband of GaN QWs as $|n, r, k\rangle =$
57 $\sqrt{2/a} \sin(\pi n z/a) e^{i\vec{k}\cdot\vec{r}} / \sqrt{L_x L_y}$, the square of the un-
58 screened intra-subband IR matrix element of scattering
59 from initial momentum state $\mathbf{k}_i(k_i, \theta)$ to a final momen-
60 tum state $\mathbf{k}_f(k_f, \theta')$ in the m^{th} subband can be written
61 as

$$|v_{IR}(q_x)|^2 = \frac{m^2}{L_x} \left(\frac{\pi^2 \hbar^2 \Delta}{m^* a^3} \right)^2 \frac{2\sqrt{2}\Lambda}{2 + (q_x \Lambda)^2} \delta_{q_y, 0}, \quad (1)$$

62 where, $\mathbf{q} = \mathbf{k}_f - \mathbf{k}_i$, L_x and L_y are the macroscopic
63 lengths of the QW in x and y directions, $\delta_{(\dots)}$ is Kronecker
64 delta function and \hbar is the reduced Planck constant. The
65 problem of IR scattering is well known and has been in-
66 vestigated for two and one dimensional electron gases in
67 many semiconductors, including nitrides. What is new
68 in non-polar structure is the polarization induced bound

a) akonar@nd.edu

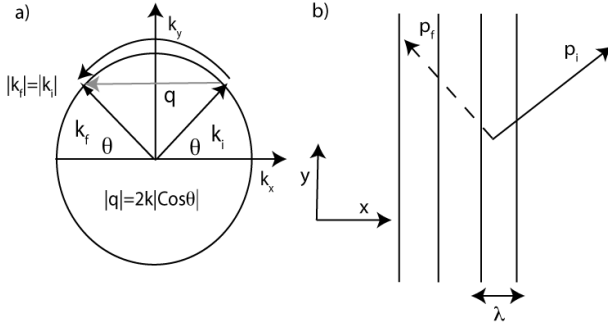


FIG. 2. schematic diagram of momentum change in anisotropic elastic scattering. a): momentum space. Clearly transverse wave vector (k_y) of carriers parallel to line charges is conserved while the net momentum change is $|2k \cos \theta|$, b) in real space electron's movement is shown.

charges associated with each interface roughness step. The thickness modulation of QW leads to GaN/AlN heterojunctions at each roughness center as depicted in Fig.1 b). The difference of in-plane polarization of GaN and AlN creates line-charge dipoles by inducing fixed charges at opposite faces of each step (as shown in Fig.1.b). Assuming each rough step is infinitely extended along the y direction (see ref. 6-9), the electrostatic potential at any point \mathbf{r} (x, y, z) in the QW arising from a polarization line-charge dipole of a roughness step at a point ($x_i, 0$) of height $\Delta(x_i)$ and lateral width d is given by

$$V(x, y, z) = v_+(x, y, z) - v_-(x, y, z) = \frac{e\lambda\pi}{4\pi\epsilon_0\kappa} \left[\ln \frac{(x - x_i - d/2)^2 + z^2}{(x - x_i + d/2)^2 + z^2} \right], \quad (2)$$

where e is the electron charge, ϵ_0 is the free-space permittivity, κ is the relative dielectric constant of GaN and $\lambda_\pi(x_i) = |P_{GaN} - P_{AlN}| \Delta(x_i)/e$ is the effective line charge density. Note that, the potential is independent of y due the symmetry of the problem. The scattering matrix element of transition from state $|n, r, k_i\rangle$ to state $|m, r, k_f\rangle$ can be written as $v(x_i, q) = \langle m, r, k_f | v(x, y, z) | n, r, k_i \rangle$, where

$$v(x_i, q) = \left(\frac{e\lambda\pi}{\epsilon_0\kappa|q_x d|} \right) e^{-iq_x x} \sinh \left(\frac{|q_x d|}{2} \right) F_{nm}(q_x a) \times \delta_{q_y, 0}. \quad (3)$$

In the above equation, $F_{nm}(q_x a)$ is the form factor arising from the quasi-2D nature of the electron gas. For our choice of the envelope function, the form factor can be calculated analytically. It approaches unity ($F_{nm}(q_x a) \rightarrow 1$), both for long wavelength ($q \rightarrow 0$) as well as for a very thin QW ($a \rightarrow 0$).

Eq. (3) represents the Fourier-transformed electrostatic potential from a line charge dipole associated with a single roughness step. As two steps are correlated, the dipole potential arising from them are also correlated. If there are N numbers of roughness steps, the square of

the matrix element of the dipole potential summed over all scatterers is given by

$$|v_{dip}(q_x)|^2 = v(0, q)^2 L_x n_{dip} \left[1 + \frac{2\sqrt{2}n_{dip}\Lambda}{2 + (q_x\Lambda)^2} \right], \quad (4)$$

where, $n_{dip} = N/L_x$ is the average roughness density (/cm) at the interface. The other two important scattering mechanisms are: i) remote charge impurity (RI) scattering, and ii) polar optical phonon scattering. To have free carriers, the QW is doped remotely. If t is the distance between the QW and the remotely doped layer, the unscreened matrix element of scattering can be written as¹³

$$|v_{RI}(q)|^2 = \left(\frac{e^2 F_{mn}(qa)}{2\epsilon_0\kappa} \right)^2 \frac{e^{-2qt}}{q^2}. \quad (5)$$

Polar optical phonon (POP) scattering rates under Davydov-Shmushkevich scheme ($\hbar\omega_0 \gg k_B T$), where phonon emission is assumed to be instantaneous, has been analytically calculated by Gelmont et. al¹⁴. The only difference between Gelmont's approach and our calculation is the form factor, which was calculated by Gelmont et. al using a Fang-Howard type wavefunction, whereas, in our case, it is calculated using infinite well (hard wall boundary conditions) -type wavefunction.

Among the scattering potentials considered above, the polarization-induced line charge potential and interface-roughness potential are anisotropic in nature. This leads to anisotropic scattering events which is captured by the Kronecker delta function ($\delta_{q_y, 0}$) appearing in the corresponding matrix elements of scattering. Fig.2 shows a typical anisotropic scattering event where, electron's momentum along y direction remains unchanged while the momentum along x direction is reversed. For such anisotropic scattering, net momentum change is $|q| \equiv |q_x| = 2k \cos \theta$, where θ is the angle of the incoming wave vector with x axis. This is in striking difference with RI scattering, where, $|q| = 2k \cos \psi$, where $\psi = \theta' - \theta$; the angle between initial and final wave vector of scattering (see inset of Fig.3b). For line charge scattering and IRs, scattering strengths are equally important at all angles except at $\theta = \pm\pi/2$ where scattering time diverges (no scattering), whereas for RI scattering only small angle scatterings rates dominate. For such anisotropic scatterers, an angle averaged single relaxation time approximation (RTA) formalism fails, and one needs to look for either variational¹⁶ or numerical solutions of Boltzmann transport equation (BTE). Recently, Schliemann and Loss¹⁷(SL) have proposed an exact solution of BTE in the presence of anisotropic scatterers which we use in this work.

To investigate the effect of anisotropic scattering events on experimentally measurable transport quantities (such as electron mobility, conductivity etc), it is sufficient to consider carrier transport along the two principal directions x and y . Transport coefficients in any arbitrary direction, in principle, can be obtained by coordinate transformation. We first consider charge transport along x .

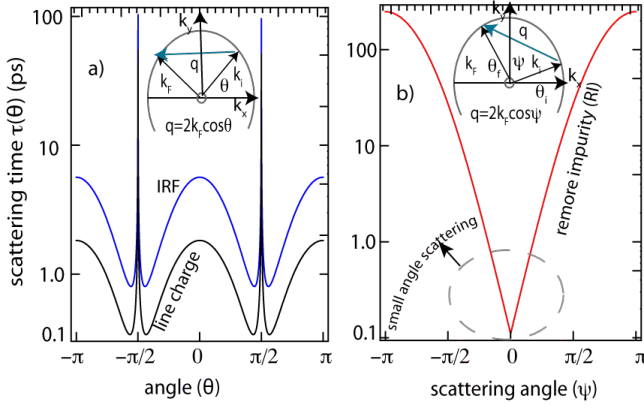


FIG. 3. a): angle (θ) dependent scattering time for line-charge (black) and IR (blue) scattering. b): RI scattering time as a function of angle (ψ) between initial and final wave vector of scattering.

153 Under the application of a small electric field $\vec{E} = (E, 0)$
 154 in the QW-plane, the non-equilibrium part of carrier dis-
 155 tribution function under the SL scheme can be written
 156 as

$$g_k^{\parallel}(\theta) = -e \left(-\frac{\partial f_0}{\partial \mathcal{E}_k} \right) A_k^{\parallel}(\theta) \mathbf{v}(\mathbf{k}) \cdot \mathbf{E}, \quad (6)$$

157 where f_0 is the equilibrium Fermi-Dirac distribution
 158 function, $\mathbf{v}(\mathbf{k})$ is the group velocity, and \mathcal{E}_k is the kinetic
 159 energy of an electron in the GaN QW. The coefficient
 160 $A_k^{\parallel}(\theta)$ is defined as

$$A_k^{\parallel}(\theta) = \frac{\tau^{\parallel}(\mathbf{k})}{1 + \left(\frac{\tau^{\parallel}(\mathbf{k})}{\tau^{\perp}(\mathbf{k})} \right)^2}, \quad (7)$$

161 where $\tau^{\parallel}(\tau^{\perp})$ is the scattering time parallel (perpendic-
 162 ular) to applied field calculated using Fermi's golden rule.
 163 Defining the current density as $\vec{J} = 2e/(L_x L_y) \sum_k g_k v_k$,
 164 the expression for mobility for a degenerate electron gas
 165 along the x direction can be calculated as

$$\mu_{xx} = \frac{e}{\pi m_{xx}^*} \int_0^{2\pi} d\theta A^{\parallel}(k_f, \theta) \times \cos^2 \theta \quad (8)$$

166 where m_{xx}^* is the electron effective mass in GaN along
 167 the c axis. A similar expression can be derived for
 168 μ_{yy} . It can be seen that for isotropic scattering, $A_k^{\parallel} =$
 169 $A_k^{\perp} = \tau(k_f)$; which leads to conventional isotropic mo-
 170 bility $\mu_{xx} = \mu_{yy} = e\tau/m^*$. In general, the integral
 171 appearing in Eq. (9) is evaluated numerically for the
 172 complicated angular dependence of the coefficient $A_k^{\parallel}(\theta)$.
 173 Nevertheless, analytical expressions of mobilities can be
 174 evaluated under certain approximation. For a very thin
 175 QW, $F_{mn}(qa) = 1$, and electron mobility for anisotropic
 176 scatterer can be written as

$$\mu_{xx}^{dip} = \frac{e\hbar\epsilon_0\kappa a_B^*}{m_{xx}^* n_{dip} (\lambda\pi d)^2} \sqrt{\frac{8n_s}{\pi^{3/2}}} \mathcal{I}_1 \left(\frac{qTF}{2k_F} \right) \quad \text{and,}$$

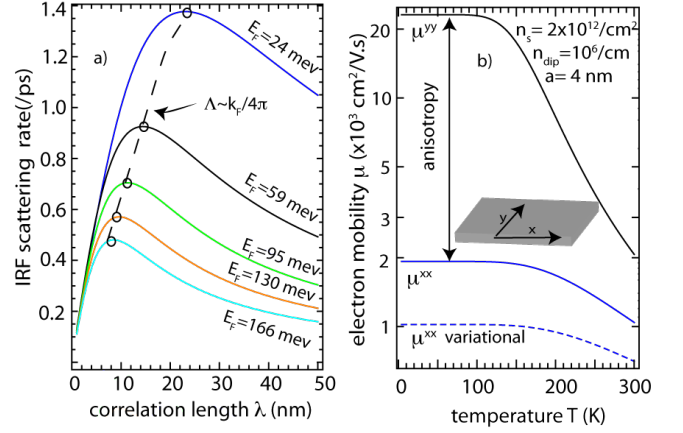


FIG. 4. a): IRF scattering vs in-plane correlation length Λ for various carrier densities (Fermi energies), b) electron mobility along two principal directions x (blue) and y (black) as a function of temperatures. The dashed blue line is the longitudinal mobility using variational technique.

$$\mu_{xx}^{IR} = \frac{ea^6}{4\hbar\Delta^2\Lambda} \sqrt{\frac{n_s}{\pi^{9/2}}} \mathcal{I}_2 \left(\frac{qTF}{2k_F} \right). \quad (9)$$

177 Where, qTF is the 2D Thomas-Fermi wave vector¹³, n_s
 178 is the equilibrium carrier density in the QW, k_F is the
 179 Fermi wave vector, and a_B^* is the effective Bohr radius¹³.
 180 The dimensionless integrals $\mathcal{I}_1 \left(\frac{qTF}{2k_F} \right)$ and $\mathcal{I}_2 \left(\frac{qTF}{2k_F} \right)$
 181 can be evaluated exactly¹⁸.
 182 For numerical calculations, a nominal set of parameters
 183 are used to describe the GaN QW roughness: $(\Delta, d) =$
 184 $(3.19, 5.2) \text{ \AA}$, whereas other parameters such as carrier
 185 density (n_s), temperature (T) and the QW thickness (a)
 186 are varied within an experimentally relevant range. An
 187 isotropic effective mass $m_{xx}^* = m_{yy}^* = 0.23m_0$ (m_0 is the
 188 mass of a bare electron) is assumed, since the effective
 189 mass along the c axis ($m_{c\parallel}^* = 0.228m_0$) and perpendicular
 190 to the c axis ($m_{c\perp}^* = 0.237m_0$) has negligible anisotropy¹⁹
 191. An important parameter describing the magnitude of
 192 roughness is the in-plane correlation length Λ . In Fig.4,
 193 we plot the IR scattering rates with in-plane correlation
 194 length Λ for different Fermi energies. The scattering rate
 195 exhibits a peak for $\Lambda \approx 1/k_x$, where IR scattering ma-
 196 trix element is maximized, and then decays slowly with
 197 Λ on either sides of the peak. For a particular scattering
 198 rate, it is possible to find two values of Λ , on each side of
 199 the peak. Since Λ is a two-valued function of scattering
 200 rates (mobility), it is necessary²⁰ to determine Λ from
 201 temperature dependent mobility data. Due to unavail-
 202 ability of transport data for non-polar GaN at present,
 203 we assume $\Lambda = 1.5 \text{ nm}$ - a typical value used¹⁵ for polar
 204 GaN HEMTs. It should be noted that the line-charge
 205 scattering rates will have similar but weaker dependence
 206 on Λ due to inclusion of correlated dipole scattering in
 207 Eq. 4.
 208 The fact that anisotropic scatterers do not hinder elec-
 209 trons moving along y direction, in principle, should result

in a higher mobility along the y direction. Fig.4b) captures this anisotropy. The temperature dependent electron mobility is evaluated along two principal directions x and y . At low temperatures, μ_{yy} , limited by RI scattering, is significantly higher than longitudinal mobility μ_{xx} which is limited by anisotropic IR and line charge scattering in addition to RI scattering. At room temperature, isotropic polar optical phonon scattering tends to reduce the anisotropy in mobility by equally affecting μ_{xx} and μ_{yy} . We have assumed distance of remote doping layer $t= 3$ nm. Larger values of t will increase the mobility anisotropy even more at low temperatures by increasing μ_{yy} exponentially. For example, a value of $t = 10$ nm would result in $\mu_{yy} \approx 10^5$ cm²/V.s²¹ for $n_s = 10^{12}$ /cm² at low temperatures; approximately 3 times higher mobility compared to $t= 3$ nm case (see Fig.4b). The dashed blue curve in Fig. 3b) shows the mobility (μ_{xx}) calculated using the variational principle^{16,22}. The difference of numerical values of mobility between variational and SL scheme stems out from the fact that variational techniques gives the lower bound of mobility.

Both line-charge and IR scattering matrix elements are strong decreasing functions of electron's kinetic energy, which implicitly depends on the magnitude of the momentum transfer q_x in scattering processes. For a degenerate electron concentration the mobility is effectively determined the carriers at Fermi level. Hence $q_x \approx 2k_f = \sqrt{2\pi n_s}$, where n_s is the equilibrium carrier density. As a result, both IR and line charge scattering rates decrease, which in effect, reduces mobility anisotropy with increasing carrier density n_s as illustrated in Fig.5a). Similarly, for wide QWs, IR ($\mu_{IR} \sim a^6$) and line charge scattering are unimportant and polar optical phonon scattering is the dominant scattering mechanism. Consequently, μ_{xx} and μ_{yy} tend to approach to the same limiting value (determined by the POP scattering rate), and mobility anisotropy is completely washed out (see Fig.5b)) for $a > 8$ nm. At this point, we want to stress upon the fact that in our numerical calculations, we have used a minimal set of parameters for interface roughness ($\Delta, d \sim$ monolayer). In practice, values of these parameters differ from sample to sample and experimentally extracted set of parameters should be used for a more accurate quantitative description of transport anisotropy. Two effects have not been taken account in our model - i) scattering from charged BSFs and ii) anisotropic strain at GaN/AlN interface. While scattering from charged BSFs is expected to enhance transport anisotropy in addition to the anisotropy presented here, strain-induced piezoelectric polarization will alter transport anisotropy by altering bound line charge density at each roughness step. How to incorporate these two effects in our model remains an open problem and should be addressed in future for a more complete and accurate description of charge transport in non-polar GaN QWs.

In summary, a theory of charge transport in non-polar GaN QWs has been presented. We show that extended defects, together with the in-plane polarization of non-

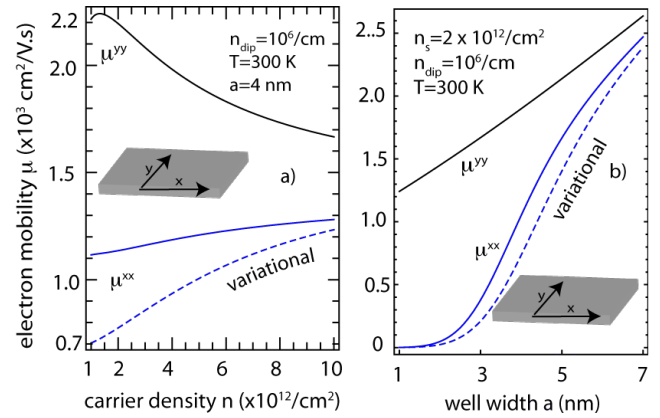


FIG. 5. electron mobility along two principal axes x (blue) and y (black)— a) as a function of carrier densities and b) as a function of well width. Note that mobility anisotropy decreases with increasing carrier density or well width. Dashed blue curves represent longitudinal mobility calculated using variational technique.

polar GaN-based devices act as anisotropic scattering centers. At low temperatures, the mobility shows highly anisotropic behavior for thin QWs. At room temperature, the magnitude of transport anisotropy is reduced by strong isotropic polar optical phonons scattering. It is shown that variational technique overestimates the transport anisotropy compared to exact solution of BTE. The authors would like to acknowledge J. Verma, S. Ganguy (University of Notre Dame) for helpful discussions and National Science Foundation (NSF), Midwest Institute for Nanoelectronics Discovery (MIND) for the financial support for this work.

- ¹P. Waltereit *et al.* Nature **406**, 865 (2000).
- ²B. A. Haskell *et al.*, J. Electron. Mater. **34**, 357 (2005).
- ³T. Fujiwara *et. al* Appl. Phys. Exp. **2**, 011001 (2009).
- ⁴Y. J. Sun *et al.*, J. Appl. Phys. **92**, 5714 (2002).
- ⁵O. Brandt, Y. J. Sun and L. Dweritz and K. H. Ploog, Physica E (Amsterdam) **23**, 339 (2004).
- ⁶L. Lymperakis and J. Neugebauer, Phys. Rev. B. **79**, 241308 (2009).
- ⁷A. Hirai *et al.*, Appl. Phys. Lett. **90**, 121119 (2007).
- ⁸H. Wang *et. al*, Appl. Phys. Lett. **84**, 499 (2004).
- ⁹T. Paskova *et. al*, J. Crystal Growth **281**, 55 (2005).
- ¹⁰C. Q. Chen *et. al*, Appl. Phys. Lett. **81**, 3196 (2002).
- ¹¹M. McLaurin, T. E. Mates, F. Wu and J. S. Speck, J. Appl. Phys. **100**, 063707 (2006).
- ¹²K. H. Baik *et al.*, IEEE. Photonics Letters **22**, 595 (2010).
- ¹³J. Davis, *Physics of Low Dimensional Semiconductors: An Introduction* (Cambridge University), Cambridge, England, 6th Ed.
- ¹⁴B. L. Gelmont, M. Shur and M. Stroschio, J. Appl. Phys. **77**, 657 (1995).
- ¹⁵Y. Cao and D. Jena, Appl. Phys. Lett. **90**, 182112 (2007).
- ¹⁶Y. Zheng *et al.*, Journal of the Physical Society of Japan **72**, 2568 (2003).
- ¹⁷J. Schliemann and D. Loss, Phys. Rev. B **68**, 165311 (2003).
- ¹⁸Defining $u = q_{TF}/2k_F$ and $v = 4k_F\Lambda$, the integral $\mathcal{I}_1(u) = \int_{-1}^1 dx|x|(|x|+u)^2/\sqrt{1-x^2} = 4/3 + 3\pi u + 6u^2$ and $\mathcal{I}_2(u) = \int_{-1}^1 dx|x|(|x|+u)^2(1+vx^2)/\sqrt{1-x^2} = 4/3+u(\pi+2u)+\frac{v}{60}(64+45\pi u+80u^2)$.
- ¹⁹I. Vurgaftman and J. R. Meyer, J. Appl. Phys. **94**, 3675 (2003).

³¹⁰ ²⁰H. Sakaki *et al.*, Appl. Phys. Lett. **51**, 1934 (1987).

³¹¹ ²¹C. Wood and D. Jena, *Polarization Effects in Semiconductors:*
³¹² *From Ab Initio Theory to Device Applications* (Springer), NY,

³¹³ USA.

³¹⁴ ²²N. W. Ashcroft and D. Mermin, *Solid State Physics*
³¹⁵ (Brooks/Cole), England.